Journal of Magnetism and Magnetic Materials 331 (2013) 156–161

Contents lists available at SciVerse ScienceDirect

Journal of Magnetism and Magnetic Materials

journal homepage: www.elsevier.com/locate/jmmm

Large enhancements of magnetic anisotropy in oxide-free iron nanoparticles

Todd C. Monson [a], Eugene L. Venturini [a], Valeri Petkov [b], Yang Ren [c], Judith M. Lavin [a], Dale L. Huber [a,*]

[a] Sandia National Laboratories, Albuquerque, NM 87185, USA
[b] Department of Physics, Central Michigan University, Mt. Pleasant, MI 48859, USA
[c] Advanced Photon Source, Argonne National Laboratory, 9700 S. Cass Avenue, Argonne, IL 60439, USA

ARTICLE INFO

Article history:
Received 1 November 2011
Received in revised form
27 July 2012
Available online 23 November 2012

Keywords:
Iron
Nanoparticle
Superparamagnetism
Anisotropy
Pair distribution function

ABSTRACT

Magnetic characterization of spherical, oxide-free, bcc iron nanoparticles synthesized with β-diketone surfactants has been performed. The results of this characterization, which included particles with diameters ranging between 2 and 5 nm show that the nanoparticles have an average anisotropy of $1.9\times10^6\pm0.3\times10^6$ J/m^3, which is more than an order of magnitude greater than the magnetocrystalline anisotropy of bulk iron. Despite their unusually large anisotropy, these particles can have saturation magnetizations of up to 210 A m^2/kg (slightly lower than bulk iron). High-energy X-ray diffraction data indicates that the Fe particles have a distorted bcc lattice, which could, at least in part, explain the magnetic behavior of these nanoparticles. Dipolar coupling between particles, while present, is weak and cannot account for the high anisotropy of these nanoparticles.

1. Introduction

Understanding the differences between nanoparticle and bulk magnetism is a major challenge, particularly when in contact with strongly interacting surfactants. Many phenomena not detected in bulk materials manifest themselves on the nanoscale and have important implications to the harnessing of magnetic nanocomposites in practical applications. Developing an understanding of magnetism in iron nanoparticles, particularly surfactant-coated and chemically-synthesized nanoparticles, is particularly difficult because the iron surface is highly reactive and easily oxidizes. A number of research groups have synthesized high-quality iron nanoparticles, but they typically have an oxide layer present on the surface and/or strongly interacting ligands. As a result, these nanoparticles are reported to have saturation magnetizations (σ_{sat}) well below that of bulk iron [1–5]. One recent publication does report very high σ_{sat} values for small iron nanoparticles that exceed the bulk value and have an effective anisotropy greater than bulk [6]. These results are instructive in attempting to understand our own results and are further discussed below.

In this paper, spherical iron nanoparticles synthesized with a β-diketone surfactant (2,4-pentandione) are characterized using superconducting quantum interference device (SQUID) magnetometry and high-energy X-ray diffraction. This synthesis of iron nanoparticles is based on the thermal decomposition of iron pentacarbonyl, where careful control of the iron precursor to surfactant ratio allows the synthesis to yield bcc iron nanoparticles with diameters ranging from 2 to 10 nm. Air-free chemistry and sample preparation techniques have been followed in order to ensure that no oxide layer is present on the surface of the nanoparticles throughout their characterizations. A more detailed description of the nanoparticle synthesis, in addition to characterization data, is presented elsewhere [7].

Due to the use of a surfactant that binds less strongly to the iron surface than ligands commonly used, nanoparticles smaller than 5 nm in diameter with β-diketone surfactants have σ_{sat} values as high as 210 A m2/kg (for bulk iron σ_{sat}=222 A m2/kg at 0 K) [8]. A magnetization curve of a 5 nm iron nanoparticle sample (size determined by transmission electron microscopy) is displayed in Fig. 1. By measuring the σ_{sat} of the sample as a function of temperature from 300 K to 5 K, we can perform a minor extrapolation to determine the 0 K σ_{sat} value, allowing comparison to common 0 K literature values. Based on the determination of the mass of Fe in this sample we calculate the σ_{sat} of the sample at 0 K to be 210 A m2/kg. Despite the bulk-like σ_{sat} values, our characterization shows that these nanoparticles have an effective anisotropy that is more than an order of magnitude greater than bulk iron. Surprisingly, this high magnetic anisotropy is constant within the range of diameters characterized (2–5 nm), an unexpected result in a system where surface effects might be expected to dominate magnetic properties. In an attempt to understand the origins of this anomalous behavior, we collected high-energy X-ray diffraction (XRD) data to examine the atomic-scale structure of the nanoparticles.

2. Experimental procedures

Both DC magnetization and AC susceptibility (χ) measurements were completed on a Quantum Design MPMS-7 SQUID

* Corresponding author. Tel.: +1 505 844 9194; fax: +1 505 284 7778.
E-mail address: dlhuber@sandia.gov (D.L. Huber).

0304-8853/$ - see front matter © 2012 Elsevier B.V. All rights reserved.
http://dx.doi.org/10.1016/j.jmmm.2012.11.026

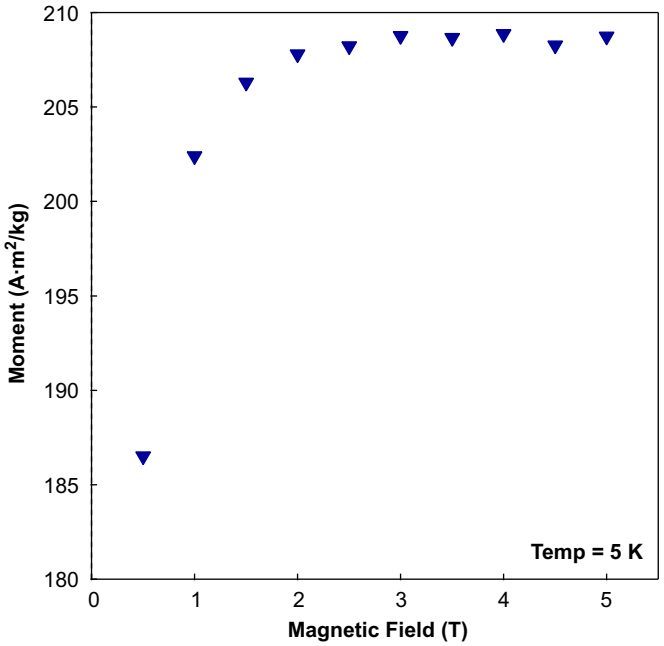

Fig. 1. Magnetization curve of an iron nanoparticle sample measured to be 5 nm in diameter through transmission electron microscopy (TEM). Based on the determination of the mass of Fe in this sample we estimate the σ_{sat} of the sample (at 0 K) to be 210 A m2/kg.

magnetometer using samples of 1 wt% iron or less dispersed in frozen solvent (dioctyl ether). Temperature sweeps were performed by zero-field cooling the sample and then measuring the magnetic moment as a function of temperature under the influence of a weak magnetic field (1 mT) during warming and subsequent cooling. AC magnetic susceptibilities were measured using an AC field of 0.35 mT and no DC field component. Precise masses for each sample were determined destructively, by forming the phenanthroline/Fe^{2+} complex, and spectrophotometrically quantifying the concentration of a known dilution [9]. Magnetic data plotting, analysis, and fitting were performed using Igor Pro (WaveMetrics, Inc., Lake Oswego, OR, USA).

High-energy X-ray diffraction experiments were carried out on beamline 11-ID-C at the Advanced Photon Source (APS), Argonne National Laboratory using X-rays of energy 114.496 keV (λ=0.1083 Å) and a two dimensional detector (mar345 image plate). For the diffraction measurements, iron nanoparticles in dioctyl ether were sealed in glass capillary tubes under an inert atmosphere. The high flux from the synchrotron radiation X-ray source allowed us to measure the weak diffraction patterns of our iron nanoparticles with very good statistical accuracy. Additionally, the higher energies of synchrotron X-rays made it possible to reach higher scattering vectors (Q). Both the high flux and ability to reach high Q are necessary for the success of the pair distribution function (PDF) analysis described later [10]. The X-ray data reduction and conversion to atomic PDFs was completed using the program RAD [11]. Structure modeling was performed using the program PDFFIT [12].

3. Results and discussion

The first indication that the iron nanoparticles studied had anomalously high magnetocrystalline anisotropies were their measured DC blocking temperatures (T_B), which were almost two orders of magnitude higher than what similarly sized nanoparticles with bulk iron's magnetocrystalline anisotropy would have. The T_B is the temperature at which a superparamagnetic particle's moment can reorient itself with the applied field in the timescale of the experiment. From the Néel–Brown model for the relaxation of magnetic nanoparticles, it can be shown that blocking temperature depends on the product of the nanoparticle volume and anisotropy [13]. For the magnetometer's DC measurement time (τ) of 100 s (which is typical for most instruments), the T_B for nanoparticles with cubic anisotropy follows the following equation:

$$T_B = \frac{K_1 V}{4k_B \ln(100/\tau_0)} \quad (1)$$

where K_1 is the first coefficient of magnetocrystalline anisotropy, V is the particle volume, k_B is the Boltzmann constant, and τ_0 is a constant referred to as the attempt time which should fall with the accepted range of 10^{-9}–10^{-12} s [13–18]. Fig. 2 displays zero-field cooled (ZFC) curves measured using DC magnetometry for iron nanoparticles with diameters of 2.3, 3.1, 3.4, and 4.5 nm (as determined by fitting the field dependent magnetometry data with a Langevin function and confirmed with TEM). Within the figure, moments are normalized for ease of comparison between data from different samples. Values of T_B can be recorded by determining the peak location in each ZFC curve. The values of T_B scale with the volume of the particles as Eq. (1) would indicate. Blocking temperatures from this DC magnetometry data are plotted as a function of particle diameter in Fig. 3. A dashed line of blocking temperatures resulting from a constant K_1 and τ_0=10^{-10} s is co-plotted with measured values of T_B and provided as a guide. These DC blocking temperatures are compared to a curve displaying the calculated blocking temperatures for hypothetical bcc Fe nanoparticles with a measurement time (τ) of 100 s, a value of τ_0=10^{-10} s, and the bulk value of K_1 for bcc iron. In all cases, T_B (and therefore K_1) for the synthesized Fe nanoparticles are well above those calculated using the values of bulk Fe. The measured blocking temperatures also lie along a line of constant anisotropy, suggesting that this anomalous property is not dominated by either surface effects (which would be

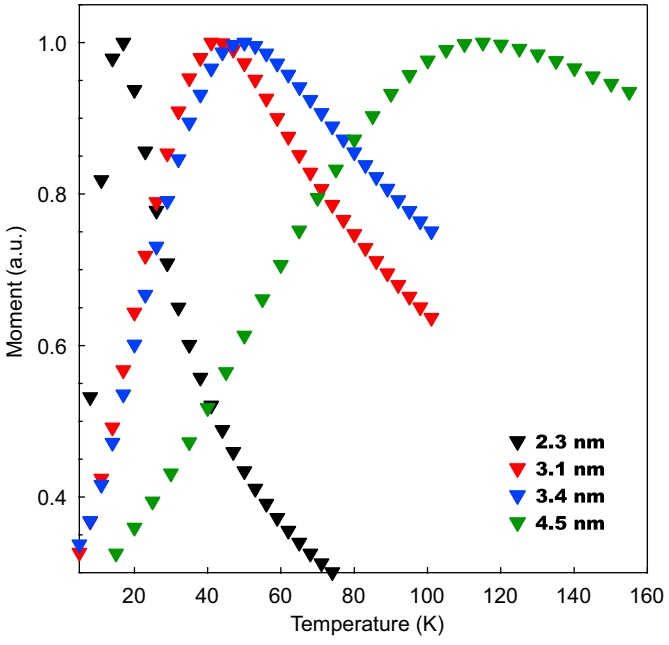

Fig. 2. ZFC curves measured using DC magnetometry for nanoparticles with diameters of 2.3, 3.1, 3.4, and 4.5 nm. The moments for each curve are normalized for ease of comparison.

strongest in the smallest nanoparticles) or dipolar interactions (which should increase with larger particle diameters).

Next, AC magnetometry experiments were performed on all four samples of iron nanoparticles. The AC susceptibilities were measured in a series of zero field cooled (ZFC) curves at the following frequencies: 0.1, 0.3, 1, 3, 10, 30, 99.9, 300, and 997 Hz. Real (a) and imaginary (b) AC susceptibilities for a 2.3 nm diameter iron nanoparticle sample are displayed in Fig. 4. To improve readability, only five frequencies are plotted. From these curves we can determine the blocking temperature for the nanoparticle sample as a function of the frequency of the applied field. In AC ZFC data, the experiment time is dictated by the frequency of the applied field, unlike DC ZFC data, where the time to reorient is the timescale of the experiment. Once again, we take T_B to be the peak moment in the ZFC data set.

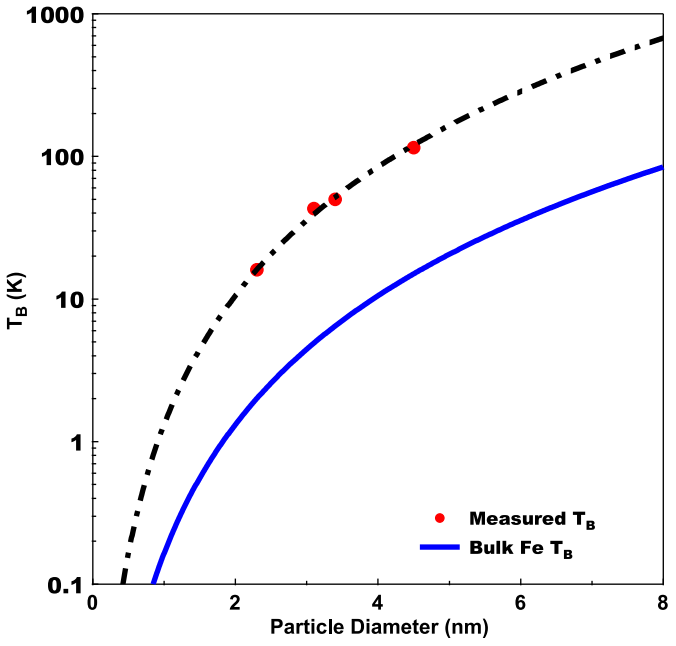

Fig. 3. Plot of T_B vs. particle diameter for a series of Fe nanoparticles of different sizes. A dashed line of blocking temperatures resulting from a constant K_1 and $\tau_0=10^{-10}$ s is co-plotted with measured values of T_B and provided as a guide. These blocking temperatures are compared to a curve (solid line) displaying what theory would predict for bcc Fe nanoparticles assuming a measurement time (τ) of 100 s, a value of $\tau_0=10^{-10}$ s, and the bulk value of K_1 for bcc iron.

Our AC data shows that the T_B increases with the measurement frequency, as expected in a thermally activated process. If the particles are assumed to be noninteracting, they should obey the Néel–Brown model, and the relaxation time (τ) can be plotted as a function of $1/T_B$ and fit with the following Arrhenius function [14,19]:

$$\tau = \tau_0 \exp\left(\frac{E_B}{k_B T}\right) \tag{2}$$

where τ_0 is the attempt time, E_B is the activation energy required to reverse a particle's magnetization, k_B is the Boltzmann constant, and T is the temperature in Kelvin (in this case T_B). E_B is equal to the product of the first coefficient of magnetocrystalline anisotropy (K_1) and the particle's volume (V) in the case of a material with uniaxial anisotropy. In the case of cubic anisotropy where the easy directions lie along the cube edges (as in bcc iron), K_1 should be replaced by $K_1/4$ [13,14].

A plot of the natural logarithm of the relaxation time vs. $1/T_B$ for the set of 3.1 nm diameter iron nanoparticles is displayed in Fig. 5. From the slope of a linear fit (dashed line) to this data we determined the particles have a K_1 value of $7.7\times10^6 \pm 0.4\times10^6$ J/m^3, which is over two orders of magnitude greater than the value for bulk iron (4.8×10^4 J/m^3) [13]. From the Y-intercept, we determined that $\tau_0=4.1\times10^{-20}\pm0.2\times10^{-20}$ s, which is too small to have physical meaning and far outside of the typical values of τ_0 (10^{-9}–10^{-12} s) [13–18]. Values of K_1 and τ_0 determined for the remaining samples (along with their mean diameters) are listed in Table 1. In all cases, K_1 is more than an order of magnitude higher than the magnetocrystalline anisotropy for bulk iron. However, since all of the determined values for τ_0 are well below the typically accepted range, the validity of the Néel–Brown model and the assumption of non-interacting particles in our samples is brought into question.

To understand and quantify the degree to which the measured magnetic properties have been perturbed by dipolar couple we have analyzed the data using several relevant approaches, including determining the model-independent empirical parameter Φ, modeling as a power-law spin glass, and finally fitting as interacting particles using the Vogel–Fulcher law.

First, to determine whether our samples were exhibiting spin-glass type behavior or that of interacting superparamagnetic nanoparticles we assessed the value of the model-independent empirical parameter Φ. This parameter relates the shift in the temperature of the maximum in χ' or χ'' (T_M) with the measured frequency, f, for an AC susceptibility data set using the following

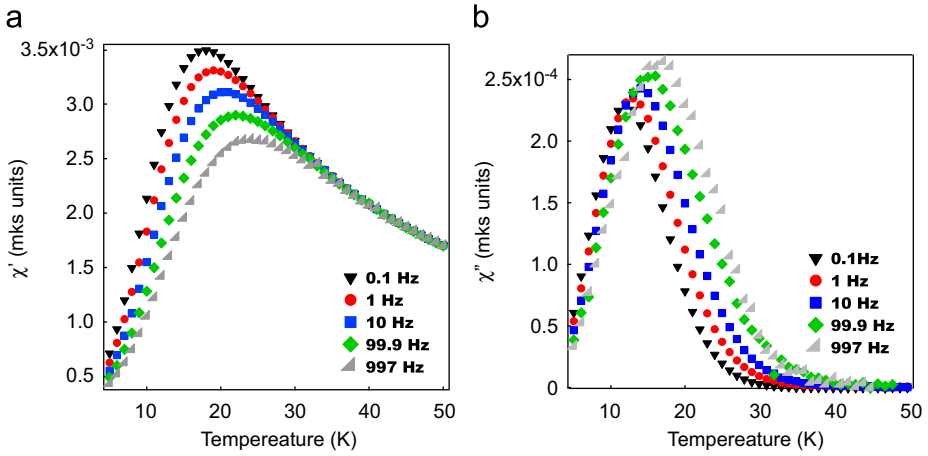

Fig. 4. Real (a) and imaginary (b) AC magnetic susceptibilities (χ) of a 2.3 nm diameter iron nanoparticle sample. Data was also collected at 0.3, 3, 30, and 300 Hz but are not displayed.

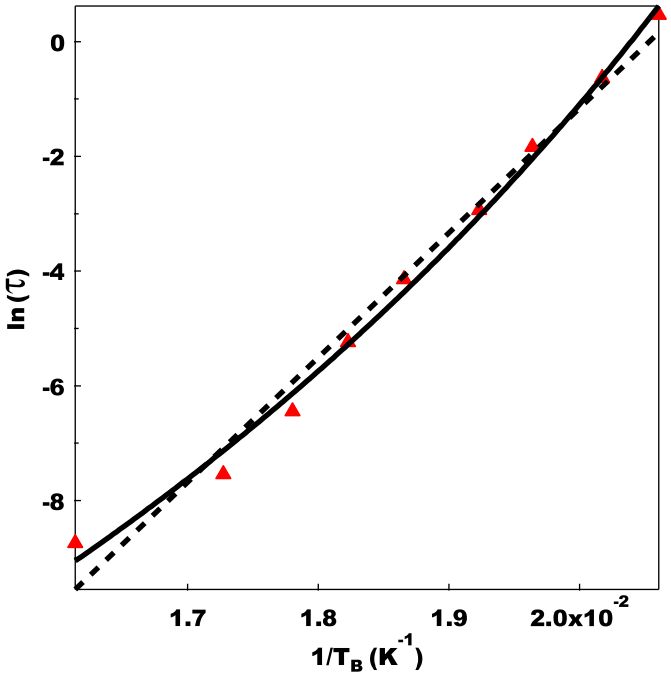

Fig. 5. Plot of the natural logarithm of the measurement frequency (f) vs. $1/T_B$ for a 2.3 nm diameter iron nanoparticle sample. The data are fit with the Néel–Brown model described by Eq. (2) (dashed line) and the Vogel–Fulcher law (solid line).

Table 1
Fitted parameters for both the Néel–Brown and spin-glass power-law models along with values of Φ evaluated about $f=30$ Hz.

Sample		Néel-Brown		Spin-Glass Power-Law		
Diameter (nm)	Φ	τ_0 (s)	K_1 (10^6 J/m^3)	τ_0 (s)	T_g (K)	zv
2.3	0.08	1.1×10^{-14}	3.4 ± 0.1	1.3×10^{-4}	8.6 ± 0.2	10.2
3.1	0.06	4.1×10^{-20}	7.7 ± 0.4	6.5×10^{-7}	39.8 ± 1.7	9.6
3.4	0.06	5.9×10^{-20}	6.6 ± 0.2	1.6×10^{-6}	40.7 ± 11.3	13.5
4.5	0.05	5.2×10^{-25}	8.0 ± 0.4	3.4×10^{-6}	111.9 ± 11.6	5.5

equation:

$$\Phi=\frac{\Delta T_M}{T_M\Delta\log(f)} \tag{3}$$

For this set of samples, Φ was evaluated about $f=30$ Hz (therefore the value of T_M at $f=30$ Hz was used). The values of Φ (also displayed in Table 1) for all of the iron nanoparticle samples lies within the range for interacting superparamagnetic nanoparticles (0.05–0.13), with a trend toward smaller values as the particle diameter increases [20]. This trend toward smaller values indicates that the degree of dipolar interaction increases with the particle size; however, values of Φ remain larger than those found in conventional spin glass systems (0.005–0.015) [21,22].

Although the values of Φ suggest that T_M is varying with respect to changes in the measurement frequency more than in a spin-glass system, fitting the data with a spin-glass model could provide additional assurance that these nanoparticle systems are not acting collectively as a spin glass. The data was fit with a model based on dynamical scaling near a phase transition, in this case, near the glass transition temperature, T_g. The equation describing this power-law behavior is

$$\tau=\tau_0\left[\frac{T_M}{T_g}-1\right]^{-zv} \tag{4}$$

where once again, τ_0 is the attempt time, and T_M is the temperature of the maximum in χ' or χ'' [22,23]. The product exponent zv is called the dynamical exponent. Fitting of the nanoparticle data with this power-law (plots not shown but fitting results are listed in Table 1) yielded good quality fits, however the values determined for τ_0 bring into question the validity of a spin glass model for these Fe nanoparticle systems. Although all of the values found for the dynamical exponent (except for the 3.4 nm particle) are within the accepted range of values (4–12) [22], the values of τ_0 are all many orders of magnitude larger than the expected values (10^{-10}–10^{-14}) [16]. Because of these unphysical large values of τ_0 the existence of a phase transition to a glassy state in our samples can be discounted.

While a spin glasslike state does not exist in the iron nanoparticle samples considered here, it is clear that there is a degree of dipolar interactions between the individual nanoparticles comprising each sample. The Vogel–Fulcher law accounts for dipolar interactions by including a term T_0, which is the strength of the particle interaction (in K). The relaxation time is defined in the following manner using the Vogel–Fulcher law:

$$\tau=\tau_0\exp\left[\frac{E}{k_B(T-T_0)}\right] \tag{5}$$

All terms except for T_0 are identical to the terms defined in the Néel–Brown model or Eq. (2). A plot of the Vogel–Fulcher model fit to the AC susceptibility data for the 3.1 nm sized sample can be seen in Fig. 5 (solid line). This sample had a value of K_1 equal to $1.8\times10^6\pm0.4\times10^6$ J/m^3, $\tau_0=1.3\times10^{-11}\pm0.1\times10^{-11}$ s, and $T_0=28.8\pm3.2$ K. For all four sizes of iron nanoparticles, the Vogel–Fulcher model yielded excellent fits and the results can be seen in Table 2. As the diameter of the particles increased, their magnetocrystalline anisotropy remained constant, with a mean value of $1.9\times10^6\pm0.3$ J/m^3. The degree of particle interaction (T_0) increased as the particles' diameter became larger, which is to be expected. However, the values of τ_0 remained within an acceptable range of physical values. The only sample for which a questionable value of τ_0 was measured was the 4.5 nm sample, whose value ($5.1\times10^{-14}\pm1.7\times10^{-14}$ s) was outside of the most accepted range of (10^{-9}–10^{-12} s) [13–15,17,18]. Other authors do suggest that reasonable values of τ_0 could be as low as 10^{-14} s [16,21]. It is clear that from the value of T_0 (65.4 ± 25.4 K) and from its value of Φ discussed earlier, that this sample has the largest degree of dipolar interactions. The value of Φ for this sample (0.05) suggests that this particle has dipolar interactions strong enough that it is on the verge of becoming a weakly coupled spin-glass. For this reason, the Vogel–Fulcher law may not provide as good of a fit as with the other three Fe nanoparticle samples, which the larger errors of the fitted parameters suggest. Nevertheless, this sample's value of K_1 ($2.1\times10^6\pm1.5\times10^6$) is no larger than the three smaller samples.

A mean value of $K_1=1.9\times10^6$ J/m^3 for all the nanoparticle samples studied gives them a magnetocrystalline anisotropy over an order of magnitude greater than the value for bulk iron (4.8×10^4 J/m^3) [13]. Since the Vogel–Fulcher law accounts for dipolar interactions, the large anisotropy cannot be attributed to particle–particle interactions. If the large anisotropy was caused

Table 2
Parameters determined through fitting AC magnetometry data with the Vogel–Fulcher law.

Diameter (nm)	τ_0 (s)	K_1 (10^6 J/m^3)	T_0 (K)
2.3	3.0×10^{-12}	2.2 ± 0.9	2.8 ± 2.3
3.1	3.1×10^{-10}	1.4 ± 0.6	30.7 ± 4.4
3.4	1.3×10^{-11}	1.8 ± 0.4	28.8 ± 3.2
4.5	5.1×10^{-14}	2.0 ± 1.6	65.5 ± 25.4

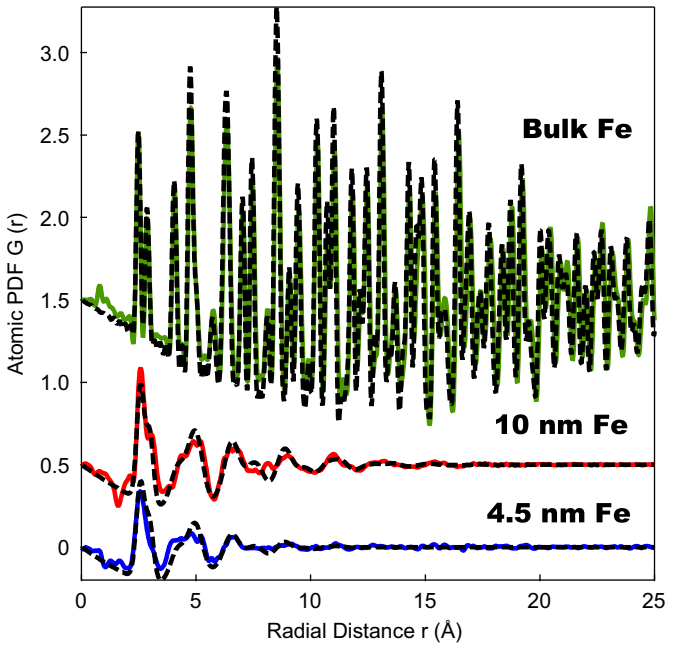

Fig. 6. Experimental atomic PDF for a micron sized (bulk) iron sample and two iron nanoparticle samples. Model PDFs are displayed as a dashed black line.

by a surface mediated effect, the values of K_1 should vary inversely with the particle diameter, but this was not the case. This lack of variation with size led us to explore the possibility that the enhanced anisotropy may be caused by some intrinsic material property of the nanoparticles.

In an effort to understand the anomalous anisotropy in these iron nanoparticles, we studied their atomic-scale structures using high-energy X-ray diffraction, analyzing the data using the PDF approach. The plots of the experimental atomic PDF as a function of radial distance and the curves generated from structure modeling appear in Fig. 6. The models were based on the crystal structure of bcc Fe. We studied three samples: micron sized (bulk) Fe, 10 nm diameter Fe nanoparticles, and 4.5 nm diameter nanoparticles. The results from the modeling of the data appear in Table 3. Both of the nanoparticle samples have a correlation length much less than their diameters, indicating that the bcc-type atomic ordering is not maintained across the entire nanoparticle. Both nanoparticle samples also have an expanded nearest neighbor distance and higher root-mean-square fluctuations in their atomic positions than bulk bcc iron. These results indicate that the nanoparticles have an expanded and distorted bcc-type structure.

We believe the distortion of the bcc-type structure, and expansion of the nearest neighbor Fe–Fe distance is, at least in part, related to the anomalous anisotropy in the iron nanoparticles. An isotropically expanded crystalline iron lattice would be expected to induce a higher magnetocrystalline anisotropy, though the magnitude of the expected increase is not clear [24]. Any breaking of the local cubic symmetry would naturally cause an even greater anisotropy increase. While the results of our modeling, shown in Fig. 6, use an isotropic distortion of the lattice, the solution is not unique, and further study is necessary to reveal the nanoparticle's structure in detail.

Ab initio calculations may be the best way to determine whether the observed expansion in Fe–Fe distances and substantial structural disorder explain the anomalously high anisotropy measured. Absent this modeling, we cannot definitively state that this is the case, but the evidence points to this conclusion. Other possible explanations including dipolar interactions, surface anisotropy, and shape anisotropy do not appear to be the dominant

Table 3
Results from modeling PDF X-ray diffraction data of one bulk and two nanoparticle iron samples. The two nanoparticle samples are labeled according their diameters.

Sample	Fe–Fe distance (Å)	Correlation length[a]	RMS atomic position fluctuation (Å^2)[b]
Bulk Fe	2.48(1)	1mm	0.005
10 nm Fe	2.56(2)	2nm	0.052
4.5 nm Fe	2.56(2)	1nm	0.052

[a] The correlation length is estimated by the distance at which the experimental PDFs decay to zero.
[b] RMS atomic fluctuations are estimated by a Gaussian fit to the first peak in the experimental PDFs. Note in bulk Fe they are mostly due to thermal disorder.

causes of the enhanced anisotropy. Both surface anisotropy and dipolar interactions are strongly size dependent, and are inconsistent with our observation of size-independent anisotropy. Surface anisotropy is enhanced in smaller particles due to the high surface to volume ratio. Conversely, dipolar interactions are very strongly dependant on particle size, with the strongest effects seen in large particles and concentrated samples [25]. Additionally, the Vogel–Fulcher law treatment of the data should have accounted for the effects of dipolar interactions. Finally, shape anisotropy cannot provide the large anisotropy enhancements we observe. Using standard approaches to calculate shape anisotropy [13], we calculate that the maximum shape anisotropy for a prolate iron spheroid is less than 1×10^6 J/m^3, which is only about half of the effect observed. For the spherical particles discussed here, with aspect ratios of less than 1.1, the effect of shape anisotropy is only on the order of 10^4 J/m^3 and is therefore negligible.

The structural changes of the iron nanoparticles we see are reminiscent of a recent publication by Margeat et al. that attributed high anisotropy in iron nanoparticles to a polytetrahedral structure [6]. While this system is qualitatively similar, the K_1 reported is considerably lower than seen in the current study (5.2×10^5 J/m^3 vs. 1.9×10^6 J/m^3). It is tempting to assume the structure observed here must similarly be polytetrahedral, but our PDF data was reproduced well by a distorted bcc model, and our pair distribution function bears no resemblance to the one published by Margeat et al. Still, there is precedent for high anisotropy in iron nanoparticles being caused by structural changes.

Other effects must be causing our particles to have a lower σ_{sat} than bulk iron since an expanded Fe–Fe distance should lead to a higher magnetic moment per iron atom [26]. Because the smaller particles have lower σ_{sat} values than the larger particles, it is likely that quenching of the surface magnetism is causing the decrease in σ_{sat}. Further experiments are underway to investigate the effect of different surfactants on both the magnetic and crystalline properties of Fe nanoparticles.

In conclusion, we have shown that chemically-synthesized iron nanoparticles with pentanedione surfactants have σ_{sat} values only slightly less than bulk iron, yet have anisotropies more than an order of magnitude greater than bulk iron. This anomalous magnetic anisotropy remains constant with respect to particle size. Results of PDF analysis of synchrotron XRD data are consistent with having a distorted bcc-type structure and a longer nearest neighbor distance than bulk bcc iron, which we believe to be at least in part responsible for the large magnetic anisotropies in these particles.

Acknowledgments

The authors are grateful to P. Provencio for her assistance with electron microscopy and J. Hatch along with B. Frankamp for their

assistance in sample preparation. Sandia National Laboratories is a multi-program laboratory managed and operated by Sandia Corporation, a wholly owned subsidiary of Lockheed Martin Corporation, for the U.S. Department of Energy's National Nuclear Security Administration under contract DE-AC04-94AL85000. This work was supported by the Division of Materials Sciences and Engineering, Office of Basic Energy Sciences, United States Department of Energy. Use of the Advanced Photon Source was supported by the U.S. Department of Energy, Office of Science, Office of Basic Energy Sciences, under Contract no. DE-AC02-06CH11357.

References

[1] N.A.D. Burke, H.D.H. Stover, F.P. Dawson, Magnetic nanocomposites: preparation and characterization of polymer-coated iron nanoparticles, Chemistry of Materials 14 (2002) 4752–4761.
[2] D. Farrell, S.A. Majetich, J.P. Wilcoxon, Preparation and characterization of monodisperse Fe nanoparticles, Journal of Physical Chemistry B 107 (2003) 11022–11030.
[3] D.L. Huber, Synthesis, properties, and applications of iron nanoparticles, Small 1 (2005) 482–501.
[4] G. Kataby, M. Cojocaru, R. Prozorov, A. Gedanken, Coating carboxylic acids on amorphous iron nanoparticles, Langmuir 15 (1999) 1703–1708.
[5] G. Kataby, Y. Koltypin, A. Ulman, I. Felner, A. Gedanken, Blocking temperatures of amorphous iron nanoparticles coated by various surfactants, Applied Surface Science 201 (2002) 191–195.
[6] O. Margeat, F. Dumestre, C. Amiens, B. Chaudret, P. Lecante, M. Respaud, Synthesis of iron nanoparticles: size effects, shape control and organisation, Progress in Solid State Chemistry 33 (2005) 71–79.
[7] D.L. Huber, E.L. Venturini, J.E. Martin, P.P. Provencio, R.J. Patel, Synthesis of highly magnetic iron nanoparticles suitable for field structuring using a beta-diketone surfactant, Journal of Magnetism and Magnetic Materials 278 (2004) 311–316.
[8] D.R. Lide, CRC Handbook of Chemistry and Physics, 82nd ed., CRC Press Boca Raton, FL, 2001.
[9] ASTM E394-00, Standard Test Method for Iron in Trace Quantities Using the 1,10-Phenanthroline Method, Annual Book of ASTM Standards, 2000.
[10] T. Egami, S.J.L. Billinge, Underneath the Bragg Peaks, Pergamon Press, Amsterdam, 2003.
[11] V. Petkov, RAD, a program for analysis of X-ray diffraction data from amorphous materials for personal computers, Journal of Applied Crystallography 22 (1989) 387–389.
[12] T. Proffen, S.J.L. Billinge, PDFFIT, a program for full profile structural refinement of the atomic pair distribution function, Journal of Applied Crystallography 32 (1999) 572–575.
[13] B.D. Cullity, C.D. Graham, Introduction to Magnetic Materials, 2nd ed., John Wiley & Sons, Inc., Hoboken, 2009.
[14] A. Aharoni, Introduction to the Theory of Ferromagnetism, 2nd ed., Oxford University Press, Oxford, 2007.
[15] A.H. Morrish, The Physical Principles of Magnetism, IEEE Press, New York, 1972.
[16] J. Souletie, J.L. Tholence, Critical slowing down in spin-glasses and other glasses—fulcher versus power law, Physical Review B 32 (1985) 516–519.
[17] V.B. Barbeta, R.F. Jardim, P.K. Kiyohara, F.B. Effenberger, L.M. Rossi, Magnetic properties of Fe_3O_4 nanoparticles coated with oleic and dodecanoic acids, Journal of Applied Physics 107 (2010).
[18] M.F. Hansen, P.E. Jonsson, P. Nordblad, P. Svedlindh, Critical dynamics of an interacting magnetic nanoparticle system, Journal of Physics—Condensed Matter 14 (2002) 4901–4914.
[19] L. Neel, Influence des Fluctuations Thermiques sur Laimantation de Grains Ferromagnetiques Tres Fins, Comptes Rendus de l'Académie des Sciences 228 (1949) 664–666.
[20] J.L. Dormann, D. Fiorani, E. Tronc, Magnetic relaxation in fine-particle systems, Advances in Chemical Physics 98 (1997) 283–494.
[21] J.L. Dormann, L. Bessais, D. Fiorani, A dynamic study of small interacting particles—superparamagnetic model and spin-glass laws, Journal of Physics C: Solid State 21 (1988) 2015–2034.
[22] J.A. Mydosh, Spin Glasses: An Experimental Introduction, Taylor & Francis, London, 1993.
[23] C. Djurberg, P. Svedlindh, P. Nordblad, M.F. Hansen, F. Bodker, S. Morup, Dynamics of an interacting particle system: evidence of critical slowing down, Physical Review Letters 79 (1997) 5154–5157.
[24] S. Ostanin, J.B. Staunton, S.S.A. Razee, C. Demangeat, B. Ginatempo, E. Bruno, Ab initio search for a high permeability material based on bcc iron, Physical Review B 69 (2004) 064425.
[25] S.A. Majetich, M. Sachan, Magnetostatic interactions in magnetic nanoparticle assemblies: energy, time and length scales, Journal of Physics D—Applied Physics 39 (2006) R407–R422.
[26] I.M.L. Billas, A. Chatelain, W.A. deHeer, Magnetism of Fe, Co and Ni clusters in molecular beams, Journal of Magnetism and Magnetic Materials 168 (1997) 64–84.